Microsphere-based short-wavelength recombination x-ray laser

E. J. Valeo and S. C. Cowley
Princeton Plasma Physics Laboratory, P.O. Box 451, Princeton, New Jersey 08543
(Received 8 April 1992; revised manuscript received 29 July 1992)

We describe a scheme for obtaining very short wavelengths ($\lambda \sim 10$ Å) in recombination lasers. The rapid cooling rates necessary to achieve population inversion during recombination are attained by adiabatic expansion of submicrometer spheres. The lasing region is made up of many such spheres. The spheres are heated impulsively by a powerful picosecond laser. First, they ionize, then as they expand, they cool and recombine. We have calculated the optimum sphere size and initial temperature for maximum gain in the $n = 3$ to 2 transition of hydrogenlike ions of elements with atomic numbers, Z, between 10 and 30. Gain of about 250 cm^{-1} is calculated in aluminum at 38.8 Å. Gain rapidly decreases with Z so that gain in titanium at 13.6 Å is about $10\,\mathrm{cm}^{-1}$. We have calculated the required pump-laser intensity and found it to be attainable with current lasers. The propagation of the pump through the "gas" of spheres is considered and the problems arising from pump scattering by the spheres are discussed.

PACS number(s): 42.55.Vc, 42.60.Da, 42.70.Hj

I. INTRODUCTION

X-ray laser development is proceeding at a rapid rate. Since the demonstration of lasing action at x-ray wavelengths in 1984 [1–3] there has been steady progress in many areas, including achievement of increased gain-length products and progression to shorter wavelengths. The future holds the promise of widespread application of these systems to areas as diverse as microlithography, microscopy, and holography[4].

We propose here a method of achieving recombination-pumped gain at lasing wavelengths of order 10 Å. The laser is similar to other recombination-pumped devices that operate successfully at longer wavelengths insofar as a high-temperature plasma is created by irradiation of a target medium with a so-called pump laser. Subsequently, the nonequilibrium conditions required for lasing are achieved by cooling the plasma sufficiently rapidly to reach a "superionized" state–one in which the ionization stage exceeds that achievable under steady-state conditions at the ambient density and temperature.

Production of the strongly nonequilibrium conditions required for gain in recombination-pumped x-ray lasers becomes problematic at short wavelengths. A picosecond cooling rate is desirable for lasing at wavelengths approaching 10 Å. This rate can be achieved with adiabatic expansion of submicrometer-sized targets. The rate cannot be achieved with radiative cooling in a single-species plasma. The fastest adiabatic cooling rate is achieved in a spherical expansion (three-dimensional expansions cool faster than two- or one-dimensional expansions). There are, in fact, three main reasons why we expect small spherical targets to be optimal. First, as we have said, they have the highest adiabatic cooling rates and therefore the highest gains. Second, small spheres have a large surface area to volume ratio and thus require less pump-laser intensity to heat. Third, submicrometer spheres are relatively easy to fabricate compared to, for instance, submicrometer fibers.

In Sec. II we calculate gain in expanding isothermal spheres. The isothermal assumption is justified by the short thermal conduction time. A simple similarity model of the hydrodynamic expansion and a collisional radiative model of the atomic physics are used. The initial temperature T_0, the initial radius R_0, and the atomic number Z of the sphere are inputs to our calculation. We calculate the gain g_{32} in the $n = 3$ to 2 transition of the hydrogenlike ion. By varying T_0 and R_0, we find the optimum values for maximum gain. The maximum of g_{32} for a given element Z is plotted in Fig. 7. The pump laser must heat the sphere to the initial temperature in a fraction of the expansion time, i.e., in a fraction of a picosecond. The required pump-laser intensity is calculated to be attainable with currently available subpicosecond lasers (see Fig. 10).

While spherical targets provide an ideal cooling geometry, they do not, of course, provide an ideal lasing geometry. The lasing region should be long enough to provide a gain length product of perhaps 10. It must also be narrow enough to be optically thin to the "dump" transition for the lower lasing level which, in our case, is the $n = 2$ to 1 transition. In aluminum these requirements yield the optimum lasing region to be about 400 μm long and 6 μm across. This geometry can be accomplished with multiple submicrometer targets, "microspheres," suspended in a vacuum or low-density gaseous medium. Perhaps the simplest method of suspending the spheres is to give them sufficient kinetic energy that their pressure supports them against gravity. The "gas" of microspheres is arranged to have a mean mass density equal to the mean mass density of a single microsphere at the time of peak gain. Clearly the optimum size of the microspheres and their spacing can be obtained from the single sphere calculations. The microsphere gas is placed in the focus of the pump laser. The focal region defines the lasing geometry; see Fig. 1. The pump laser will propagate in the

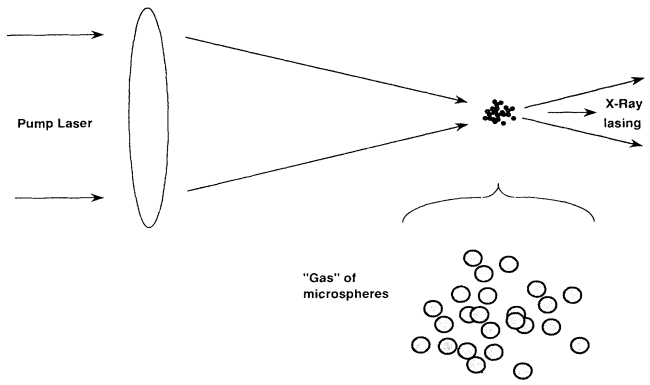

FIG. 1. Lasing geometry showing focal region defining elongated gain structure.

microsphere gas with some scattering and absorption. At high Z the scattering makes the simple pumping scheme of Fig. 1 inappropriate (see Sec. III E). Other pumping geometries are therefore suggested for high Z. Thus, with the appropriate pump intensity, spheres in the focal region are heated to the optimum temperature for gain. The heated spheres expand and fill the space, forming a relatively uniform high-gain region. Our design raises the possibility of efficient generation of shorter wavelengths than are currently available.

In Sec. II, we consider the evolution of a single sphere of initial temperature T_0 and radius R_0. The hydrodynamic similarity model of the expansion is discussed in Sec. II A. In Sec. II B, we present a simple model of the atomic physics to aid understanding. The full computational model is presented in Sec. II C. In Sec. III, we discuss the heating by the pump laser and the propagation of the pump laser in the microsphere gas. The isothermal assumption is justified in Sec. III A. The absorption and scattering of the pump laser by the spheres is calculated in Sec. III B. In Sec. III C, we calculate the required pump intensity. The physical constraints on the size and shape of the lasing region are calculated in Sec. III D. Finally we calculate the propagation of the pump laser in Section III E. In the conclusion we discuss future work and other applications of the microsphere "gas."

II. GAIN IN A SINGLE SPHERE

In this section we consider the evolution of a single sphere and the gain achieved in the evolution. We shall calculate the optimum values of the initial sphere radius R_0 and initial temperature T_0 for maximum gain. The gain g_{32} in the $n = 3$ to 2 transition in hydrogenlike ions is calculated. In Sec. II A we consider the hydrodynamic evolution of a sphere (which fortunately decouples from the atomic physics). A simple analytic calculation of the atomic physics is presented in Sec. II B. This calculation is not quantitatively accurate, but it does show the scaling trends and it does aid our understanding. Results from the model are summarized in Fig. 3. There we plot the maximum value of g_{32} and the values of T_0 and R_0 which maximize gain, all as a function of Z. In Sec. II C we present the computational model and our results, which are displayed in Figs. 5–8.

A. Hydrodynamic evolution of microsphere

The objective is to heat the sphere of radius R_0 to a uniform temperature T_0–which for now we specify only as being comparable to the ionization potential of that ion stage which will subsequently lase–in a time short compared to the disassembly time C_S/R_0. We shall be dealing with fully stripped ions and hydrogenlike ions with atomic numbers Z greater than 10. The *initial* sound speed C_S is therefore given by $C_S = (ZT_0/2M)^{1/2}$, where M is the mass of the ion. The electron density in a solid ($\sim 10^{24}\,\mathrm{cm}^{-3}$) greatly exceeds the critical density $n_{e,\mathrm{cr}}$, where the laser frequency ω equals the local electron plasma frequency ω_{pe}, for currently available lasers of the required intensity and pulse duration ($n_{e,\mathrm{cr}} \sim 10^{21} - 10^{22}\,\mathrm{cm}^{-3}$). Additionally, although the optimal sphere radius can be substantially smaller than the wavelength of the pump laser, it typically greatly exceeds the collisionless skin depth c/ω_{pe}. Therefore the pump laser deposits energy at the surface of the sphere in a layer of width c/ω_{pe}. The pump intensity required to deposit this energy is considered in Sec. III C. If the sphere is too large, the time for thermal diffusion from the heated surface to the center will exceed the disassembly time, with the result that the core will remain cold and relatively weakly ionized. Cold matter will absorb the x rays by bound-free transitions [5]. It is therefore desirable to keep the lasing medium relatively isothermal. In Sec. III A we show that the isothermal assumption holds for the spheres we consider. The atoms are ionized to the hydrogenlike stages very rapidly. In modeling the hydrodynamic expansion we make use of the large value of Z. The change in electron density due to the ionization from the hydrogenlike state is neglected since it produces a relative density change of order Z^{-1}. We also neglect the energy involved in ionization, recombination, and atomic transitions since it is typically a fraction Z^{-1} of the energy in free electrons. These approximations allow us to decouple the hydrodynamic problem from the atomic physics. Thus we solve the hydrodynamics for the temporal evolution of the electron density and temperature whose values are then used to compute the evolution of the atomic physics. If the plasma is allowed to freely expand into vacuum, then, after it increases its dimensions to a size substantially larger than R_0, its further evolution as a function of radius r and time t is found to be well described by a similarity solution of the hydrodynamic equations [6]. The isothermal similarity solution has a Gaussian density profile of width $R(t)$ [see Eq. (2)]. It is an *exact* solution of the hydrodynamic equations. Although the similarity solution is observed to agree with the true solution for $R(t) \gg R_0$, it is not quantitatively correct for $R \sim R_0$ (because the initial density profile is not Gaussian). Since there is really only one scale in the problem, R_0, it is expected that the behavior of the similarity solution for $R \sim R_0$ is qualitatively correct. In our numerical models we show that the maximum gain oc-

curs at $9R_0 > R \gtrsim 2R_0$ for all elements between $Z = 10$ and 30 [see Fig. 8(b)]. For simplicity we shall use the similarity model for all times, i.e., even for $R \sim R_0$. We expect this approximation to yield gain within 50% of the true gain.

Within the similarity model, the current plasma size $R(t)$, on-axis density $n(t) \equiv n(r = 0, t)$, and temperature $T(t)$ are determined in terms of their corresponding initial values R_0, n_0, and T_0 by the simple relations

$$\frac{d^2R(t)}{dt^2} = \frac{C_S^2}{R(t)} \quad , \tag{1a}$$

$$T(t) = T_0\left(\frac{R_0}{R(t)}\right)^{\lambda_T} \quad , \tag{1b}$$

$$n(t) = n_0\left(\frac{R_0}{R(t)}\right)^{\lambda_n} \quad , \tag{1c}$$

and where λ_T (λ_n) takes on the value $2d/3$ (d) with $d = 1, 2, 3$ in the case of planar, cylindrical, and spherical geometry, respectively. From Eq. (1a) we see that for $R(t) \gg R_0$, we have the simple result $R(t) \simeq R_0 C_S t$. Equation (1b) follows from the conservation of entropy in adiabatic expansion and Eq. (1c) follows from the conservation of particles. Having obtained the density evolution at the symmetry point $r = 0$, the off-axis density follows from the similarity form

$$n(r, t) = n(t) \exp\left\{-\frac{1}{2}\left[\frac{r}{R(t)}\right]^2\right\} \quad . \tag{2}$$

The radial velocity of the fluid element at (r, t) is

$$V_r(r, t) = \left[\frac{r}{R(t)}\right] C_S \quad . \tag{3}$$

B. Analytic model

In this section we will examine a simple analytic model of the atomic physics in an expanding sphere. (The quantitative results of this section differ from our more detailed numerical results, but the qualitative features are correct.) Let us consider the origin of the sphere only and let us take the long-time approximation to $R(t)$, i.e., $R(t) \simeq R_0 + C_S t$. We normalize Z to 10 (since we are interested in Z between 10 and 30), T_0 to the ionization potential E_H for the hydrogenlike ion, R to R_0, R_0 to 10^{-5} cm, and the initial density n_0 to 10^{24} cm^{-3}. Thus $Z = 10\bar{Z}$, T_0 (eV) $= 1360\bar{Z}^2\bar{T}_0$, $x = R/R_0$, R_0 (cm) $= 10^{-5}\bar{R}_0$, and n_0 (cm^{-3}) $= 10^{24}\bar{n}_0$. We also take the atomic mass number to be $2Z$. The lasing wavelength in these units is λ_{32} (Å)$= 65.6/\bar{Z}^2$. In normalized units the expansion rate is

$$\frac{dx}{dt} = \frac{C_S}{R_0} = 2.6 \times 10^{12} \frac{\bar{Z}\sqrt{\bar{T}_0}}{\bar{R}_0} \text{ sec}^{-1} \quad . \tag{4}$$

During the early stages of the expansion we require ionization to dominate so that a population of fully stripped ions is obtained. The initial electron temperature must therefore be comparable to the ionization potential of the hydrogenlike ion (i.e., $\bar{T}_0 \sim 1$). We shall assume (both for the analytic and numerical work) that initially all atoms are in the ground state of the hydrogenlike ion. In fact, at this temperature, ionization to the heliumlike state is very rapid. Ionization from heliumlike to the hydrogenlike state is roughly twice as fast as ionizing the hydrogenlike ion to the fully stripped ion. Thus a more accurate analysis would include the helium like stage.

Our simplified model for the hydrogenlike ion is illustrated in Fig. 2. The model consists of three levels in the hydrogenlike ion and the fully stripped ion. The $n = 1$ ground state has the fractional population n_1, the $n = 2$ and 3 excited levels have fractional populations n_2 and n_3, respectively, and the fully stripped ion has a fractional population n_∞. Clearly, $n_1 + n_2 + n_3 + n_\infty = 1$.

The fractional populations of the excited states n_2 and n_3 are typically much smaller than the fractional populations in the ground state n_1 and fully stripped state n_∞. This is just a result of the fact that the collisional sources for these levels are typically smaller than the radiative decay rates. The analytic model contains the following transition rates between levels $n = 1$, 2, and 3: the collisional excitation rate between $n = 1$ and 2, denoted C_{12}, the radiative transition rate between 3 and $n = 2$ (A_{32}), the radiative transition rate between $n = 2$ and 1 (A_{21}), and the collisional deexcitation rate between $n = 3$ and 2 (C_{32}). The collisional excitation from level

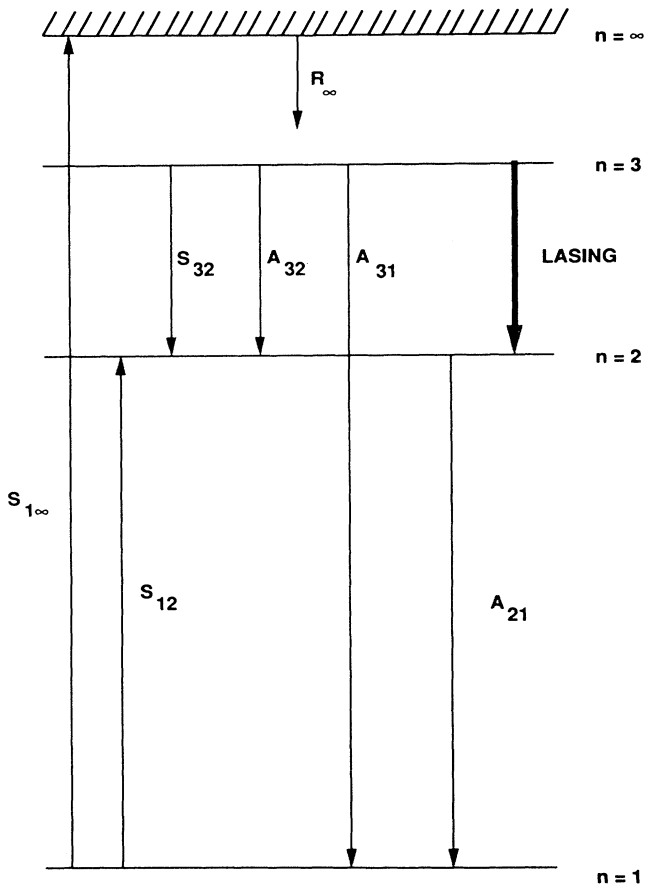

FIG. 2. Diagram of four-level laser used in analytic investigation of gain.

$n = 2$ is ignored as $n_2 \ll 1$ and the collisional deexcitation rate from $n = 2$ is unimportant compared to the radiative decay. We consider single step ionization from the $n = 1$ level only ($C_{1\infty}$). Ionization from $n = 2$ and 3 is small when the radiative rates dominate and n_2 and n_3 are populated less than the thermal equilibrium value. [In fact a numerical evaluation of $(C_{12}/A_{21})C_{2\infty}$ shows that for parameters of interest it is less than $C_{1\infty}$.] At the densities of interest ($n \sim 10^{22} - 10^{24}\,\mathrm{cm}^{-3}$) three-body recombination dominates radiative recombination. The electrons preferentially recombine into the upper levels of the atom. The upper levels are approximately in Boltzmann-Saha equilibrium with the free electrons as the collisional transition rates are high. The lower levels, however, are dominated by radiative decay. One develops a picture of a recombining electron diffusing (random walking) through the upper levels of the atom until it reaches some critical lower level. At this critical level n_c radiative decay dominates and the electron rapidly decays to the ground state. Obviously no population inversion can occur in levels above n_c because they are in Saha equilibrium. The diffusional flux of electrons through the upper levels has been calculated by many authors (see Zel'dovich [7] and Pert [8]) to be proportional to $Z^3 n^2/T^{9/2}$. In our normalized units this yields the recombination rate due to this process,

$$R_\infty = 1.3 \times 10^{11} \frac{\bar{n}_0^2}{\bar{T}_0^{9/2}\bar{Z}^6} x^3 \ \mathrm{sec}^{-1} \quad , \tag{5}$$

where we have used Eqs. (1b) and (1c) for $T(x)$ and $n(x)$. (It is interesting to note that, in the recombining plasma, the electron-ion plasma parameter is only somewhat larger than 1, especially at low Z. The modification to the recombination rate have been discussed by Biberman, Vorob'ev, and Yakubov for a strongly coupled plasma [9]. These corrections are small for the plasmas under consideration here.) We assume R_∞ gives the net recombination rate and that a fraction b of this rate gives the flux of electrons from $n > 3$ levels into the $n = 3$ level. Thus we have modeled the effect of the levels with $n > 3$ on the source for level $n = 3$. Note direct recombination into the $n = 3$ level without passing through the higher n states is relatively unimportant.

We will assume that the initial electron temperature is smaller than the $n = 2$ to $n = 1$ transition energy. The collisional rates $C_{1\infty}$ and C_{12} can be calculated using the cross sections for ionization and excitation at threshold. These cross sections are independent of energy and proportional to Z^{-4}. The rates $C_{1\infty}$ and C_{12} are obtained by averaging σv over the Maxwellian (for more complete approximations see Keane's thesis [10]). Thus in normalized units

$$C_{1\infty} \simeq 20.6 \times 10^{12} \frac{\bar{n}_0}{\bar{Z}^3\sqrt{\bar{T}_0}} \frac{1}{x^2} \exp\left(-\frac{x^2}{\bar{T}_0}\right) \mathrm{sec}^{-1} \quad , \tag{6}$$

$$C_{12} \simeq 30 \times 10^{12} \frac{\bar{n}_0}{\bar{Z}^3\sqrt{\bar{T}_0}} \frac{1}{x^2} \exp\left(-\frac{3}{4}\frac{x^2}{\bar{T}_0}\right) \mathrm{sec}^{-1} \quad . \tag{7}$$

The $n = 3$ to $n = 2$ collisional deexcitation, C_{32}, is obtained from C_{23} by detailed balance. Thus we find

$$C_{32} \simeq 25 \times 10^{12} \frac{\bar{n}_0}{\bar{Z}^3\sqrt{\bar{T}_0}} \frac{1}{x^2} \mathrm{sec}^{-1} \quad . \tag{8}$$

The mean radiative rates [11] are

$$A_{21} = 4.7 \times 10^{12} \bar{Z}^4 \ \mathrm{sec}^{-1} \quad , \tag{9}$$

$$A_{32} = 0.43 \times 10^{12} \bar{Z}^4 \ \mathrm{sec}^{-1} \quad , \tag{10}$$

and

$$A_{31} = 0.55 \times 10^{12} \bar{Z}^4 \ \mathrm{sec}^{-1} \quad . \tag{11}$$

For values of $\bar{Z}$ of interest ($\bar{Z} \sim 1.5$) the radiative rates A_{21}, A_{32} and A_{31} are larger than the expansion rate and the ionization and recombination rates. The populations of the $n = 3$ and 2 levels are therefore in quasisteady state, i.e.,

$$n_3 \simeq b n_\infty \frac{R_\infty}{(A_{32} + A_{31} + C_{32})} \quad , \tag{12}$$

$$n_2 \simeq \frac{1}{A_{21}}(A_{32} n_3 + C_{12} n_1) \, . \tag{13}$$

The ionization recombination balance in the model is

$$\frac{dn_1}{dt} = R_\infty n_\infty - C_{1\infty} n_1 \, . \tag{14}$$

Since n_2, $n_3 \ll n_1$, n_∞, we set $n_\infty = 1 - n_1$ and we use Eq. (4) to replace $d/dt = (dx/dt)d/dx$. Thus

$$\frac{dn_\infty}{dx} = -0.05 \frac{\bar{R}_0 \bar{n}_0^2}{\bar{T}_0^5 \bar{Z}^7} x^3 n_\infty + 8 \frac{\bar{n}_0 \bar{R}_0}{\bar{T}_0 \bar{Z}^4} \frac{1}{x^2} \exp\left(-\frac{x^2}{\bar{T}_0}\right)(1 - n_\infty) \, . \tag{15}$$

Typically we shall be interested in situations where $\bar{T}_0 \sim 1$ (although we have assumed $\bar{T}_0 < 1$ to derive $C_{1\infty}$ and C_{12}) and $\bar{R}_0 \sim 1$. Clearly ionization dominates Eq. (15) at $x = 1$. As the sphere expands (x increases) the ionization rate drops rapidly and the recombination rate rises rapidly. Thus the evolution splits rather naturally into two phases–the ionization phase and the recombination phase. The total fractional ionization after the ionization phase n_∞^1 can be estimated by ignoring recombination over this time. Thus

$$n_\infty^1 \simeq 1 - \exp(-\alpha) \quad , \tag{16}$$

where

$$\alpha = 8 \frac{\bar{n}_0}{\bar{T}_0} \frac{\bar{R}_0}{\bar{Z}^4} \int_1^\infty \frac{dx}{x^2} \exp\left(-\frac{x^2}{\bar{T}_0}\right) \sim 4 \frac{\bar{n}_0 \bar{R}_0}{\bar{Z}^4} \exp\left(-\frac{1}{\bar{T}_0}\right) \quad , \tag{17}$$

and we have evaluated α in the limit $\bar{T}_0 < 1$. Physically α represents the amount of ionization in the first expansion time. When $\bar{R}_0$ or $\bar{T}_0$ is small the sphere expands and cools before significant ionization occurs. During the recombination phase, typically when $x \gg \bar{T}_0$, we may ignore ionization in Eq. (15) and obtain

$$n_\infty \sim n_\infty^1 \exp -\beta \frac{x^4}{4} \quad ,$$

where

$$\beta = 0.05 \frac{\bar{R}_0 \, \bar{n}_0^2}{\bar{T}_0^5 \, \bar{Z}^7} \tag{18}$$

is roughly the amount of recombination in the first expansion time.

There is, in fact, a third phase in the evolution where ionization and recombination balance and the left-hand side of Eq. (15) is negligible (the quasistatic situtation). This occurs for parameters of interest when $\beta x^4 \gg 1$ and n_∞ is small. In the quasistatic phase

$$n_\infty \sim \frac{H(x)}{1 + H(x)} \quad , \tag{19}$$

where

$$H(x) = 160 \frac{\bar{T}_0^4}{\bar{n}_0} \bar{Z}^3 \frac{1}{x^5} \exp\left(-\frac{x^2}{\bar{T}_0}\right) \quad .$$

As we shall see, gain occurs during the recombination phase and not during this later steady-state phase. If $\beta \geq 1$ ($\bar{T}_0 \ll 1$ or $\bar{R}_0 \gg 1$), then the recombination phase does not exist–the initial ionization phase takes the ion directly into the quasistatic phase.

The gain per unit length at line center g_{ul} for a transition from level u to level l is

$$g_{ul} = \frac{S(\lambda_{ul})}{8\pi c} \frac{n_e}{Z} \lambda_{ul}^4 A_{ul} \left[n_u - n_l \frac{g_u}{g_l} \right] . \tag{20}$$

Here $S(\lambda)$ is the line-shape function, normalized so that

$$\int d\lambda \, S(\lambda) = 1 . \tag{21}$$

As we demonstrate in the Appendix, the value of $S(\lambda_{ul})$ for the lines of interest is

$$S(\lambda_{ul}) = \frac{F_{ul}}{(2\pi)^{1/2}} \frac{1}{\Delta\lambda_d} , \tag{22}$$

where the linewidth

$$\Delta\lambda_d = \lambda \frac{C_S}{c} \tag{23}$$

is due to the Doppler width caused by the expansion of the spheres [12, 13]. The factor $F_{ul} = 0.29$ for the 3→2 and 0.67 for the 2→1 transition in H-like ions. In our case, the degeneracies $g_j = j^2$. Using Eqs. (12) and (13) and the rates, Eqs. (5)–(11) we obtain

$$g_{32} \sim 4.6 \times 10^5 \frac{\bar{n}_0}{\bar{Z}^8 \bar{T}_0^{1/2} x^3} \times \left\{ \frac{\bar{n}_0^2 b x^3}{\bar{T}_0^{9/2} \bar{Z}^6} \frac{n_\infty}{Q_a} - \frac{85 \bar{n}_0}{\bar{Z}^3 \bar{T}_0^{1/2}} \exp\left(-\frac{3}{4} \frac{x^2}{\bar{T}_0}\right)(1 - n_\infty) \right\} \quad . \tag{24}$$

The first term in the braces is essentially proportional to the recombination rate, where the factor

$$Q_a \equiv \left(1 + \frac{60 \bar{n}_0}{\bar{Z}^7 \bar{T}_0^{1/2}} \frac{1}{x^2}\right) \tag{25}$$

is the "quenching coefficient," defined as the ratio of the total deexcitation rate (collisional plus radiative) to the radiative decay rate of the upper lasing level. The second term in Eq. (24) is the excitation from $n = 1$ to 2 populating the $n = 2$ level and lowering the gain. For large $\bar{T}_0$ and small x the second term dominates and the gain is negative. Since g_{32} is a monotonically increasing function of n_∞ and x it must increase during the ionization phase when n_∞ and x are increasing. Substituting Eq. (19) into Eq. (24) we see that the gain is always negative in the quasistatic phase.

We have calculated (numerically) the maximum value of g_{32} from Eq. (24), maximizing with respect to x, T_0, and R_0. In Fig. 3 we plot the maximum g_{32} as a function of Z, together with the values of R_0 and T_0 which optimize g_{32}. In these computations, we estimate b by

$$b_{\rm br} = \frac{A_{43} + C_{43}}{(A_{43} + C_{43} + A_{42} + A_{41})} \quad ,$$

which is the branching ratio into level 3 from level 4. The maximum g_{32} given by this model exceeds the numerical result of Sec. II C by a factor of 10 for $Z = 20$. However, since the model is rather simplified, numerical accuracy is not expected.

A number of qualitative features can be understood from this model. First let us consider the steep inverse scaling of g_{32} with Z. At high Z the collisional rates are small and therefore $n_3 \sim [R_\infty/(A_{32} + A_{31})]n_\infty$. Using $\Delta\lambda_d \propto \lambda Z$, $\lambda \propto Z^{-2}$, and $R_\infty \propto Z^{-6}$ and setting $n_2 \sim 0$ and $n_\infty \sim 1$ we obtain from Eq. (20), $g_{32} \propto Z^{-14}$. At low Z collisional deexcitation dominates the decay from the $n = 3$ level ($Q_a \gg 1$), thus $n_3 \sim (R_\infty/C_{32})n_\infty$ and

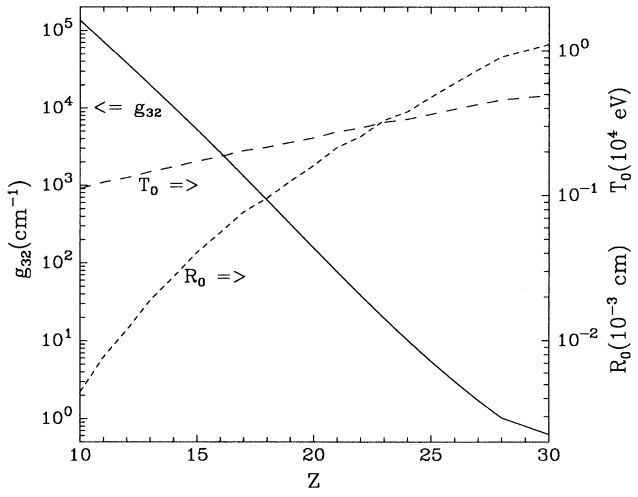

FIG. 3. Variations with atomic number Z as predicted by the analytic model. Left scale: Maximum on-axis gain g_{32} (cm^{-1}), (solid line) optimized over both R_0 and T_0. Right scale: Initial sphere radius R_0 (10^{-3} cm) (short-dashed line) and initial electron temperature T_0 (10^4 eV) (long-dashed line) which lead to maximum gain.

$g_{32} \sim Z^{-7}$. Note we have implicitly assumed that $\bar{T}_0$ and n_∞ do not scale significantly with Z; their calculated scalings are indeed mild. Clearly the dominant reasons for the strong decrease in gain with increasing Z are the scalings of R_∞ and λ.

The existence of a maximum g_{32} can be understood, again qualitatively, from our model. First consider the initial temperature $\bar{T}_0$. If $\bar{T}_0$ is small the amount of ionization and therefore gain is small. Conversely, if $\bar{T}_0$ is large, the recombination rate is always small, the $n = 1$ to 2 excitation rate is large, and the gain is consequently small. Clearly an optimal temperature exists. Now consider the initial radius $\bar{R}_0$. If $\bar{R}_0$ is small the sphere expands very rapidly and cools before significant ionization takes place. However, if $\bar{R}_0$ is large the cooling is slow and the atom is in a quasiequilibrium where $n = 1$ to 2 excitation populates the $n = 2$ level and shuts off the gain. Again we expect an optimum $\bar{R}_0$. These opposing tendencies are sketched in Fig. 4.

The advantages of spherical expansion are also apparent from our model. Clearly we hope to achieve significant initial ionization but insignificant ionization during the recombination phase. Thus one wishes to have an ionization rate and an $n = 1$ to 2 excitation rate that decrease rapidly with x and a recombination rate that increases rapidly with x. Now consider three types of symmetrical expansion: planar ($d = 1$), cylindrical ($d = 2$), and spherical ($d = 3$). The $n = 1$ to 2 excitation rate is proportional to $x^{-2d/3}\exp(-3x^{2d/3}/4\bar{T}_0)$ and therefore it decreases most rapidly with x when $d = 3$, i.e., in spherical expansion. The ionization rate behaves similarly. The recombination rate is proportional to x^d and therefore increases most rapidly (with x) when $d = 3$. Thus spherical expansion is preferable.

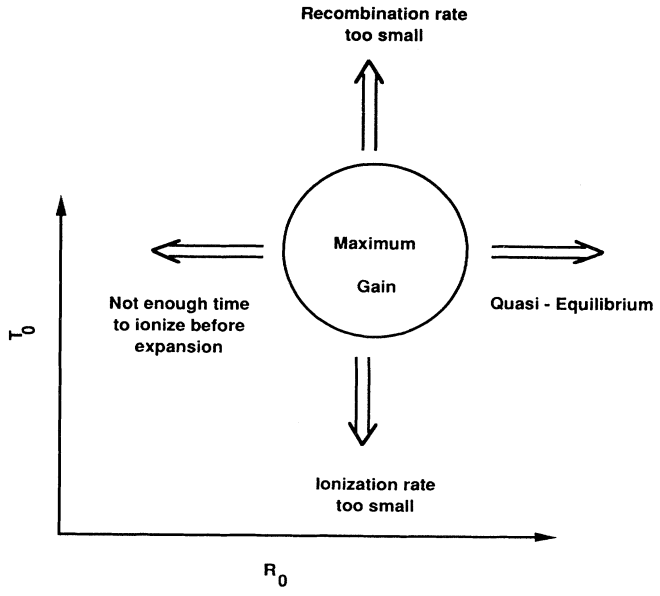

FIG. 4. Sketch illustrating competing effects which lead to a maximum in gain as a function of initial sphere radius R_0 and temperature T_0 for a given atomic number Z.

C. Numerical model

After a discussion of the numerical method, we examine in some detail the time evolution of a single sphere. This is followed by a discussion of the optimization of gain with respect to initial radius R_0 and temperature T_0, given Z. Finally, the variation of optimized gain and other critical quantitites, such as the optical depth of the dump transition, with Z are presented.

1. Numerical method

In the general case, the evolution of the atomic states and radiation fields must be kept on a par with that of the hydrodynamic variables. Fortunately, for our system the power density associated with atomic excitation and ionization is small compared to the cooling power resulting from expansion. As we stated in Sec. II A, this is a consequence of the large Z. This circumstance allows an accurate computation of the evolution in two independent steps. First, the hydrodynamic evolution is computed neglecting the power flow into internal atomic states. Then the density and temperature so computed enter as time-dependent parameters in the computation of the atomic state.

Given the time evolution of the fluid variables, the evolution of the fractional populations of the ground and excited states of the hydrogenlike ion and of the fully-stripped ion are computed in a Lagrangian frame

$$\frac{d\mathbf{r}}{dt} = \mathbf{V} \quad , \tag{26}$$

with $\mathbf{V}(\mathbf{r}(t), t)$ the local flow velocity. We neglect ionization from and recombination to lower ionization stages on the grounds that during the heating phase, collisional ionization from He-like ions will occur on a much shorter time scale whenever significant gain is achieved, and that during the recombination phase, recombination into He-like ions will not affect the gain calculations. With these remarks, the governing equations for the bound-state fractional populations are

$$\frac{dn_j}{dt} = S_j + C_j - I_j + R_j \quad . \tag{27}$$

Here

$$S_j = \sum_{j'(>j)} A_{j'j} n_{j'} - \sum_{j'(<j)} A_{jj'} n_j \tag{28}$$

is the net spontaneous transition rate into level j, expressed in terms of the individual rates $A_{j'j}$ from j' to j,

$$C_j = n_e \left[\sum_{j'(\neq j)} (C_{j'j} n_{j'} - C_{jj'} n_j) \right] \tag{29}$$

is the net rate of collisional excitation into level j from all other bound states j' expressed in terms of the rate coefficient $C_{jj'}$ from j to j',

$$I_j = n_e n_j C_{j\infty} \tag{30}$$

is the ionization rate from level j, expressed in terms of the ionization rate coefficient $C_{j\infty}$, and

$$R_j = n_e n_\infty (n_e \alpha_{tb,j} + \alpha_{rad,j}) \tag{31}$$

is the sum of the three-body and radiative recombination rates ($\alpha_{tb,j}$ and $\alpha_{rad,j}$, respectively) into level j. All sums over bound states are up to a level l which is varied to check convergence. The rate coefficents are those given by Drawin [14].

The equation for the evolution of the fractional population of fully stripped ions is

$$\frac{dn_\infty}{dt} = I_\infty - R_\infty \quad , \tag{32}$$

where

$$I_\infty = \sum_j I_j \tag{33}$$

is the total rate of collisional ionization from, and

$$R_\infty = \sum_j R_j \tag{34}$$

is the sum of recombination rates into, all bound states. By virtue of the relations Eqs. (33) and (34) and the additional evident relation

$$\sum_j C_j = 0 \quad , \tag{35}$$

we have that the total population

$$n_t \equiv \sum_j n_j + n_\infty \tag{36}$$

is conserved,

$$\frac{dn_t}{dt} = 0 \quad . \tag{37}$$

By definition $n_t = 1$.

There is a large variation in the magnitude of the rate coefficients in the set of equations (27) and (32), both with changes in temperature and in quantum number. This variation could be expected to cause difficulty in a numerical solution, but the set has been found to be amenable to accurate solution with standard scientific library algorithms [15]. The chosen algorithm conserves density to machine roundoff (10^{-15}).

Once the fractional populations are computed, the gain at line center for the 3 to 2 transition follows immediately from Eqs. (20)–(23).

2. *Time evolution*

As an illustrative example, we present results for the time evolution of a titanium sphere ($Z = 22$) in Figs. 5(a)–5(e). The initial radius of the sphere $R_0 = 2.17 \times 10^{-5}\,\mathrm{cm}$. It is assumed initially at rest $\dot{R}(t = 0) = 0$. The initial electron density on axis $n(0)$ is set to $1 \times 10^{24}\,\mathrm{cm}^{-3}$, essentially solid density. The sphere is assumed impulsively heated to an electron temperature $T_0 = 3.1 \times 10^3\,\mathrm{eV}$, equal to 0.47 of the ionization potential of the hydrogenlike ion. The sphere is then assumed to freely expand into vacuum. The evolution of the sphere size $R(t)$ is obtained by solving Eq. (1a). $T(t)$ and $n(t)$ are then obtained by evaluation of Eqs. (1b) and (1c), respectively. All three are plotted in Fig. 5(a). We note there the decrease of $T(t)$ by more than a factor of 9 in 1.5 psec.

Given the hydrodynamic evolution, the state populations are then computed as described in Sec. II C 1. We have found that inclusion of seven excited states, with principal quantum numbers $n = 2, \ldots, 8$, adequately describes the hydrogenlike system for these purposes. This was confirmed in two ways: First, sensitivity of computed gain to changes was shown to be small. Second, during the interesting time interval, the populations of all but the first four or so levels were seen to be quite close to Saha equilibirium (i.e., within $\sim 5\%$) with the free-electron fully stripped ion populations. The evolution of the fractional population of the ground state of the hydrogenlike ion n_1 and of the line-center gain at $r = 0$, g_{32}, are presented in Fig. 5(b). Ionization proceeds to a level of 12% in 320 fsec, followed by recombination with an effective rate of about $1.2 \times 10^{12}\,\mathrm{sec}^{-1}$. Upon onset of recombination, the gain rises rapidly to $11.1\,\mathrm{cm}^{-1}$ at 860 fsec and then decays at a rate comparable to the fully stripped population. Several characteristic features of these profiles persist through our scans in R_0, T_0, and Z. First, the width in time of the gain profile is comparable to the delay in its onset after impulsive heating. This has the important consequence that, in practice, producing overlap among the gain profiles of an ensemble of similar spheres is readily achievable. Second, especially at higher Z's (say above 15) the optimal maximum fractional ionization of the hydrogenlike ion is much less than unity (as was assumed in the analysis of Sec. II B). We find that for such Z values, if ionization fractions of order unity are achieved, then recombination-induced gain is much less than optimal. This is simply a consequence of the fact that, at large Z, the recombination rate drops steeply with Z [see Eq. (24)], steeper than the $n = 1$ to 2 excitation rate. Thus the normalized temperature $\bar{T}_0$ must be lowered to keep the $1 \rightarrow 2$ excitation small. The ionization rate is therefore lower because Z rises and $\bar{T}_0$ falls; see Eq. (6). The expansion rate is roughly constant at high Z. Thus the amount of ionization (in an expansion time) is reduced.

The fractional populations of the upper and lower lasing levels, n_3 and n_2, respectively, are shown in Fig. 5(c). Again, consistent with the neglect of effects of doubly excited states, fractional excitations are small.

Further diagnostics are presented in Figs. 5(d) and 5(e). There the line-center optical depth for the dump transition, defined here as $\tau_{12} \equiv g_{12}(r = 0, t)R(t)$, although initially larger than unity, is seen to drop to 0.58 at peak gain. Similarly, the quenching coefficient at $r = 0$,

$$Q(t) \equiv \frac{1}{A_{32}}[n_e(0,t)C_{32} + A_{32}] \quad , \tag{38}$$

drops to 0.46 at peak gain. Another potential gain spoiler, excitation of level 2 from the ground state, is plotted there as well. The relative excitation coefficient

represented by

$$R_{\rm ex} \equiv \frac{n_1 C_{12}}{n_2 A_{21}} \tag{39}$$

is seen to drop to 0.11 at peak gain.

We remark that separate computations of the gain off-axis ($r \neq 0$) show that, typically, regions of positive gain extend out to radii several times $R(t)$ during the time interval of appreciable gain on axis ($r = 0$). This observation indicates that the total gain per sphere $G(t) = 2\int_0^\infty g(r,t)\,dr$ is expected to be positive when the gain at $r = 0$ is. Additionally, we have found that G is well represented (to factors of order unity) by $g(r=0,t)R(t)$.

3. Optimization

Within our model the evolution is completely characterized by the parameters R_0, T_0, and Z. Optimization

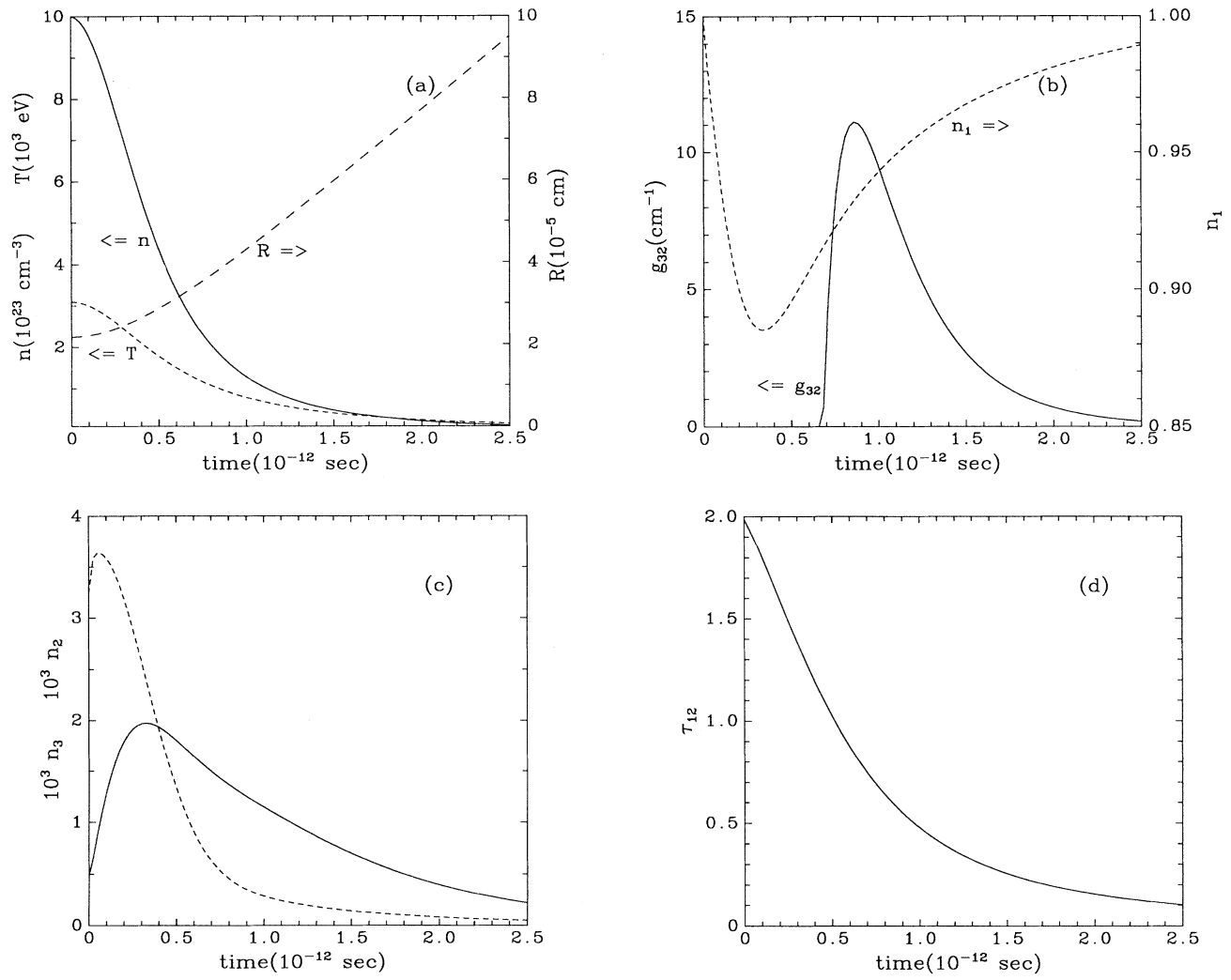

FIG. 5. Time evolution of hydrodynamic and atomic variables for titanium, $Z = 22$, which has a lasing wavelength of 13.6 Å. The initial conditions are those which yield the largest value of the maximum in $g_{32}(t)$. The initial radius $R_0 = 2.17 \times 10^{-5}$ cm. The initial electron temperature $T_0 = 3.1 \times 10^3$ eV. In all figures, the time ranges from the instant of heating (time = 0) to 2.5 psec thereafter. (a) Evolution of hydrodynamic variables. Left scale: electron density n (10^{23} cm^{-3}) (solid line), electron temperature T (10^3 eV) (short-dashed line). Right scale: sphere radius, R (10^{-5} cm), as defined through Eqs. (1a) and (2) (long-dashed line). (b) Evolution of the fractional population of the ground state n_1 of the hydrogenlike ion (dashed line) and of the line-center gain g_{32} (cm^{-1}) at $r = 0$ (solid line). (c) The fractional populations of the upper and lower lasing levels n_3 (solid line) and n_2 (dashed line). (d) The line-center optical depth τ_{12} for the dump transisiton, defined here as $g_{12}(r=0,t)R(t)$, is 2 initially, but drops to 0.58 at the time (0.86 psec) of peak gain. (e) The quenching coefficient at $r = 0$, $Q(t)$ (solid line), defined by Eq. (38), drops to 0.46 at peak gain. The importance of excitation of the lower lasing level by collisional excitation from the ground state is characterized by the relative excitation coefficient $R_{\rm ex}$ (dashed line), defined by Eq. (39), which is seen to drop to 0.11 at peak gain.

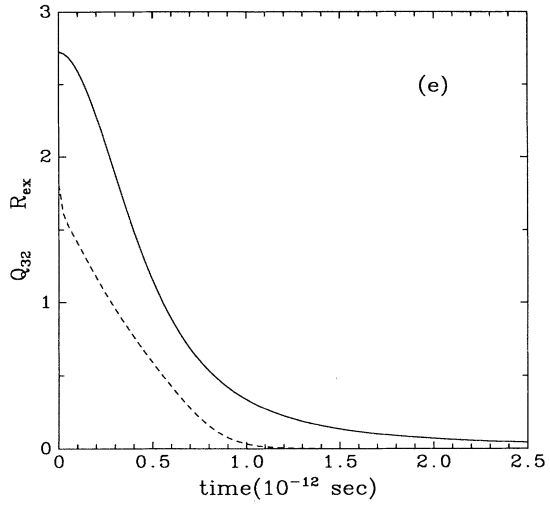

FIG. 5. (*Continued*).

of peak gain with respect to (R_0, T_0) for a given Z and determination of sensitivity of the gain profile to deviations from optimum conditions have been carried out by computing on-axis evolution for a set of initial conditions (R_0, T_0). As an example, the results for titanium are shown in Fig. 6. A single maximum in the peak gain of $11.1\,\mathrm{cm}^{-1}$ is achieved for $R_0 = 2.17 \times 10^{-5}$ cm, $T_0 = 3.1 \times 10^3$ eV. As predicted by the analytic model, we observe the competition between insufficient ionization for low initial temperatures and/or radii and insufficiently rapid recombination at large initial temperatures and/or radii.

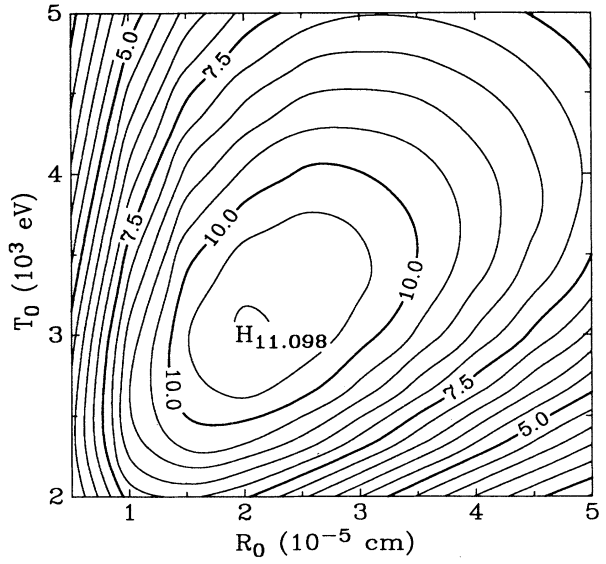

FIG. 6. Contour plot of peak gain vs initial sphere radius R_0 and electron temperature T_0, for $Z = 22$. The maximum occurs for $R_0 = 2.17 \times 10^{-5}$ cm and $T_0 = 3.1 \times 10^3$ eV, the same parameters as the evolution plots of Fig. 5.

4. Variation with atomic number

The optimization computations of Sec. II C 3 have been repeated for each Z in the range ($Z = 10$, $\lambda = 65.6$ Å) to ($Z = 30$, $\lambda = 7.29$ Å). The results are presented in Figs. 7(a)–(d). In all cases, the initial electron density was taken to be $10^{24}\,\mathrm{cm}^{-3}$. Note that since gain scales like the initial density cubed, we have not considered spheres of lower initial density. Figures 8(a)-8(d) give various important quantities at the time t^* of peak gain for each Z.

III. HEATING AND PUMP-LASER PROPAGATION

In this section we consider the requirements for a pump laser. In Sec. III A we show that the typical thermal conduction time is short and that the isothermal assumption is good. We obtain the scattering and absorption cross sections for the spheres in Sec. III B. The pump-laser intensity requirements are calculated and shown to be attainable with existing lasers in Sec. III C. The "dump transition" from level $n = 2$ to 1 must be optically thin (we assumed that it was so in Sec. II), otherwise the population of the $n = 2$ level is large and the gain is negative. In Sec. III D we discuss how this requirement limits the width of the lasing medium. Finally, in Sec. III E we discuss the pump propagation in the "gas" of microspheres and show that scattering of the pump light is problematic. We offer specific ideas how to minimize scattering or tolerate scattering.

A. The isothermal assumption

In this section we use the nondimensional units of Sec. II. We make estimates of the collisional transport of heat assuming that the sphere does not move (expand) in the times of interest. This assumption is of course justified by the fact that the calculated thermal equilibration time is short compared to the expansion time C_S/R_0. The electron collision rate in inverse seconds is $\nu_e = 2.3 \times 10^{15} \bar{n}_0 \bar{T}_0^{-3/2} \bar{Z}^{-2}$. One should note that, at the temperatures of interest, the number of electrons in a Debye sphere is large, $(4\pi/3n)\lambda_D^3 \gtrsim 100$ and $T \gg T_{\mathrm{Fermi}}$, so it is quite correct to treat the spheres as a weakly coupled plasma. Therefore electrons establish a local Maxwellian in a small fraction of the expansion time ($C_S/R_0 = 2.6 \times 10^{12} \bar{Z} \bar{T}_0^{1/2} \bar{R}_0^{-1}$). Furthermore, the electron mean free path λ_{MFP} is short compared to the radius of the sphere. Specifically,

$$\frac{\lambda_{\mathrm{MFP}}}{R_0} \sim 9 \times 10^{-2} \frac{\bar{T}_0^2 \bar{Z}^3}{\bar{n}_0 \bar{R}_0} \quad . \tag{40}$$

Thus we estimate the time to reach a uniform temperature by using the collisional transport coefficients of Braginskii [16]. In order to include some geometrical factors we choose the estimated rate to be the decay rate of the lowest-order (slowest decaying) eigenmode of the linearized heat diffusion equation ν_{iso}. Thus normalizing this rate to C_S/R_0 we obtain

$$\frac{\nu_{\rm iso} R_0}{C_S} \sim 110 \frac{\bar{Z}^3 \bar{T}_0^2}{\bar{R}_0 \bar{n}_0} \quad . \tag{41}$$

We note that the argument given above to justify the isothermal approximation applies even more strongly to the collisionless skin depth–i.e., heat diffusion over the collisionless skin depth is much faster than the time to expand a collisionless skin depth. Thus the only scale of interest in the expansion is R_0. Our estimate uses the final temperature to estimate thermal conduction and thus slightly overestimates the heat conduction. Since we have a large ratio in Eq. (41) such details are not expected to change the basic conclusion that the sphere is isothermal for all the cases of interest.

B. Pump scattering and absorption from the microspheres

We shall take a simple linear electron response to the field inside the microsphere (we treat the microsphere as a dense plasma sphere). So the current **J** is given by

$$\frac{4\pi}{c}\mathbf{J} = \frac{{\omega_{pe}}^2 \mathbf{E}}{c(\nu_e - i\omega)} \quad , \tag{42}$$

where $\omega_{pe} = (4\pi n_e e^2/m_e)^{1/2} = 5.6 \times 10^{16}\, \bar{n}_0^{1/2}\, \sec^{-1}$ is the plasma frequency, ω is the pump-laser frequency, and ν_e is the electron collision rate. Since $\nu_e = 2.3 \times$

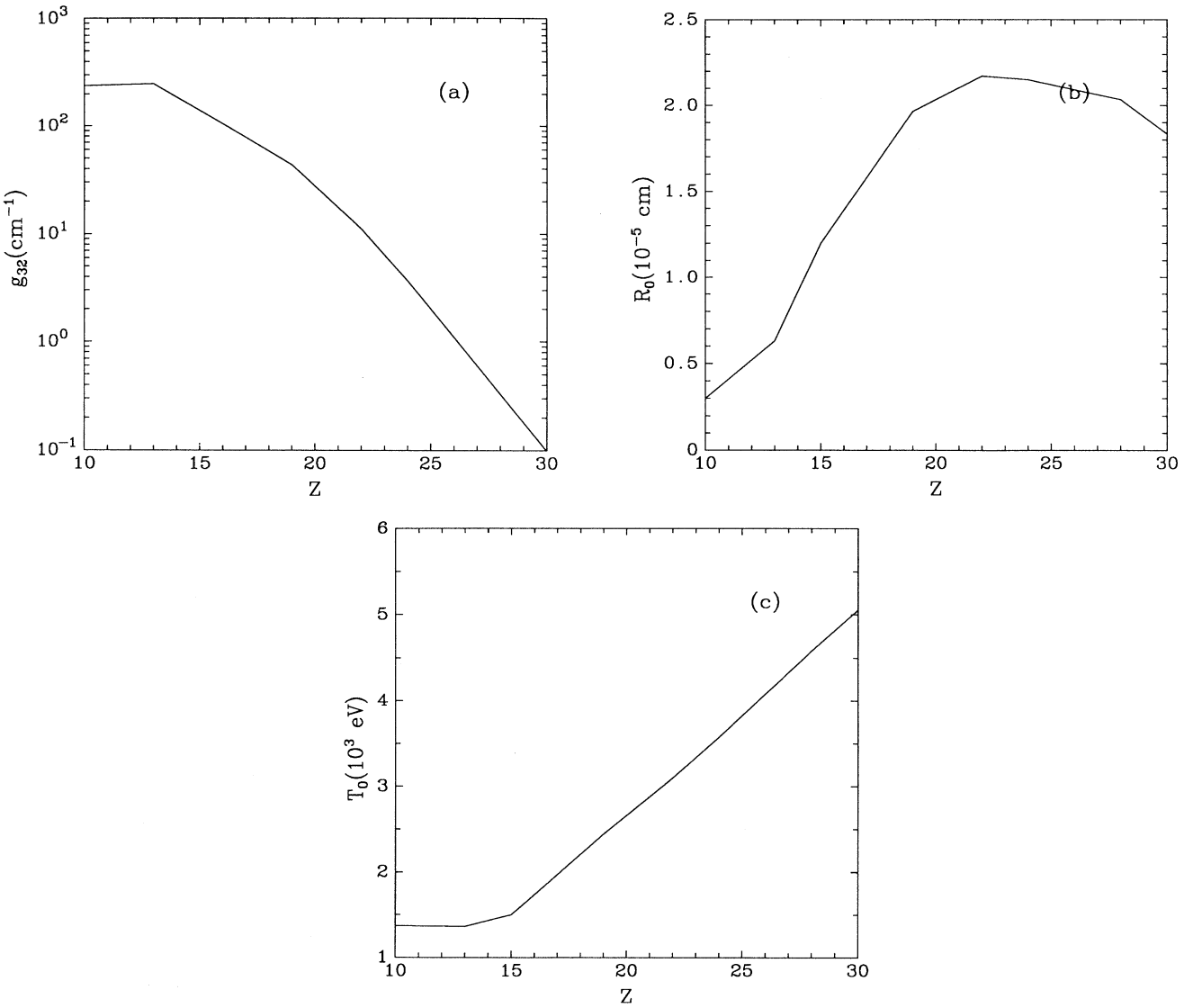

FIG. 7. Variations with atomic number Z as predicted by the numeric model. (a) Maximum on-axis gain g_{32} (cm^{-1}), optimized with respect to both R_0 and T_0. (b) Initial sphere radius R_0 (10^{-5} cm), which leads to maximum gain. (c) Initial electron temperature T_0 (10^3 eV), which leads to maximum gain.

$10^{15}\,\bar{n}_0\bar{T}_0^{-3/2}\bar{Z}^{-2}\,\mathrm{sec}^{-1}$ and a typical ω is $7.5\times10^{15}\,\mathrm{sec}^{-1}$ (as for a KrF picosecond pump laser), $\omega_{pe} \gg \omega, \nu_e$. We can therefore ignore the displacement current in Maxwell's equations and obtain

$$\nabla^2\mathbf{B} = \frac{{\omega_{pe}}^2}{c^2}\left(\frac{\omega}{\omega + i\nu}\right)\mathbf{B} \quad . \tag{43}$$

Thus the **B** field and therefore the current is confined to a layer of width l_p, the skin depth d,

$$l_p = \frac{c}{\omega_{pe}}\left|1 + \frac{i\nu}{\omega}\right|^{1/2} \quad . \tag{44}$$

Typically for $\omega \sim \nu$, $l_p \sim 4\times10^{-7}\,\bar{n}_0^{1/2} \ll R_0$ and one can consider the laser heating to be in a narrow shell on the outside of the microsphere. We therefore take the limit $l_p/R_0 \ll 1$ and $kl_p \ll 1$ where $k = \omega/c$, but we shall consider $kR_0 \simeq 1$. In this limit the sphere scatters light as if it were perfectly conducting. The absorption is small in the parameter kl_p, and results from the deviation from the perfectly conducting approximation. The calculation is standard; see, for instance Jackson [17]. Thus the scattering cross section σ_{sc} is

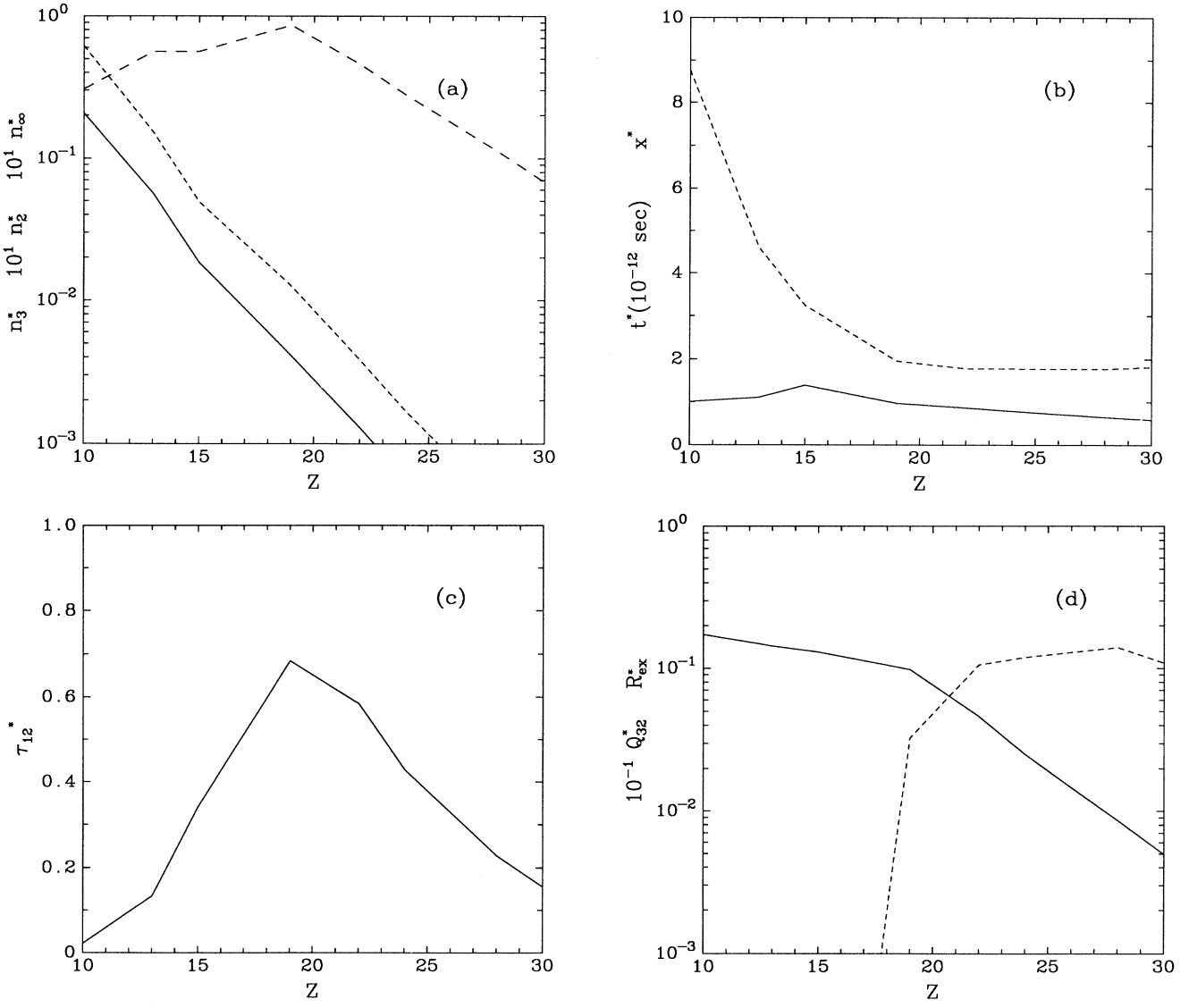

FIG. 8. Various quantities at the instant t^* of peak gain vs atomic number Z. (a) Fractional ionization n_∞^* (long-dashed line), upper n_3^* (solid line) and lower n_2^* (short-dashed line) lasing level fractional populations. (b) Time t^* (solid line) and relative expansion x^* (dashed line). (c) Opacity of dump transition $\tau_{12}^* \equiv g_{12}(r=0,t^*)R(t^*)$. (d) Quenching Q^* (solid line) and relative excitation R_{ex}^* (dashed line).

$$\sigma_{\rm sc}(x) = 2\pi R_0^2 \sum_{l=1}^{\infty}(2l+1)\frac{1}{x^2}\left\{\frac{j_l^2}{j_l^2+y_l^2} + \frac{[(l+1)j_{l-1} - lj_{l+1}]^2}{[(l+1)j_{l-1} - lj_{l+1}]^2 + [(l+1)y_{l-1} - ly_{l+1}]^2}\right\} = \pi R_0^2\, F(x) \quad , \tag{45}$$

where $x = kR_0$ and $j_l(x)$ and $y_l(x)$ are the spherical Bessel functions [18]. The absorption cross section $\sigma_{\rm abs}$ is

$$\sigma_{\rm abs}(x) = \alpha(\omega)\, 2\pi R_0^2 \sum_{l=1}^{\infty}(2l+1)\frac{1}{x^4}\left\{\frac{1}{j_l^2+y_l^2} + \frac{1}{[(l+1)j_{l-1} - lj_{l+1}]^2 + [(l+1)y_{l-1} - ly_{l+1}]^2}\right\} = \alpha\pi R_0^2\, G(x) \quad , \tag{46}$$

where

$$\alpha(\omega) = {\rm Re}\left[\frac{-\omega}{\omega_{pe}} i \left(1 + \frac{i\nu}{\omega}\right)^{1/2}\right] \quad .$$

Re indicates that we take the real part of the expression in the brackets. Clearly $\alpha(\omega)$ is small and the absorption cross section is small compared to the geometric cross section. We plot $F(x)$ and $G(x)$ in Fig. 9. Note that for $kR_0 \ll 1$, $\sigma_{\rm sc} \sim (10/3\pi)R_0^2(kr_0)^4$ (Rayleigh scattering) and $\sigma_{\rm abs} \sim 6\pi R_0^2\,\alpha(\omega)$. Thus it is possible at long wavelength for the scattering cross section to be smaller than the absorption cross section.

We remark that, insofar as scattering is concerned, the linear approximation should provide accurate results, since, even for the rather collisional solid density plasmas considered here, the absorption cross section is, in general, very small compared to the scattering cross section. Collective effects which may lead to enhanced absorption will not appreciably affect the scattering cross section unless the effective collision frequency becomes comparable to ω_{pe}, an unlikely circumstance. As for absorption, the linearized calculation should provide a conservative estimate. Calculations of the effects of collective processes on absorption, currently a subject of intensive investigation [19], are beyond the scope of this paper. Any such enhancements would reduce the constraints on the pumping geometry.

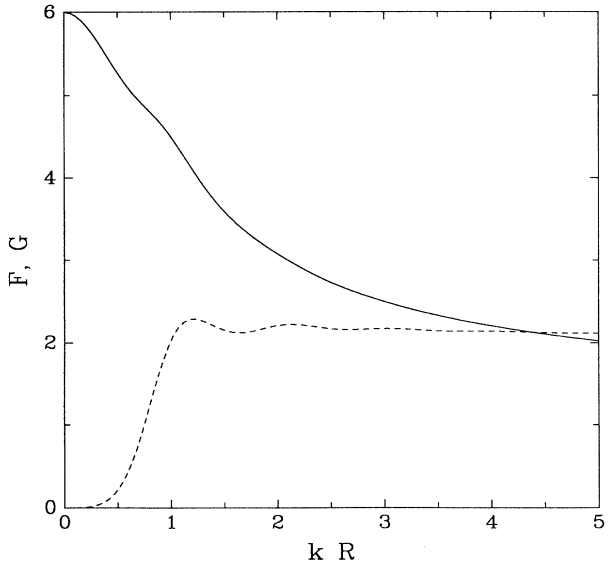

FIG. 9. Plots of single-sphere scattering function $F(x)$ (dashed line) Eq. (45) and absorption function $G(x)$ (solid line) Eq. (46) vs normalized pump-laser wave vector $x = kR$.

C. Intensity requirements for the pump laser

The pump laser must heat the sphere before expansion since one wants a hot high-density plasma initially. Thus we shall assume that the laser pulse lasts for a time at most equal to

$$\tau_{\rm pump} \equiv 0.5\frac{R_0}{C_S} \quad . \tag{47}$$

Using Eq. (46) for the absorption cross section we obtain the required laser intensity I (asuming that the energy delivered is $I\sigma_{\rm abs}\tau_{\rm pump}$), where

$$I = 2.2\times 10^{16}\,\frac{\bar{n}_0\bar{T}_0^{3/2}\bar{Z}^3}{\alpha(\omega)G(x)}\,{\rm W\,cm^{-2}} . \tag{48}$$

Note that the total energy delivered to each sphere is $\bar{Z}^2\bar{n}_0\bar{R}_0^3\bar{T}_0$ μJ. Typically $\nu_e \ll \omega$ and $\alpha \simeq \nu_e/2\omega_{pe}$. Then

$$I \simeq 5.4\times 10^{17}\,\frac{\bar{n}_0^{1/2}\bar{T}_0^3\bar{Z}^5}{G(x)}\,{\rm W\,cm^{-2}} . \tag{49}$$

When $x = kR_0 \to 0$, $G(x) \to 6$. We see that the required intensity scales very unfavorably with $\bar{Z}$. Currently available picosecond lasers can deliver as much as $10^{19}\,{\rm W\,cm^{-2}}$. In Fig. 10 we have plotted the required intensity of 0.25-μm light as a function of Z [using Eq. (48)] for the optimal sphere with $R_0(Z)$ and $T_0(Z)$ as obtained in Sec. II C. Also shown there is the corresponding maximum pump-laser pulse length $\tau_{\rm pump}$. We note that at high Z the required intensity in fact approaches $10^{19}\,{\rm W\,cm^{-2}}$. One may, therefore, be forced to use a less than optimal value of T_0 at high Z. We also note that the pulse length requirement demands state of the art picosecond lasers.

D. Constraints on lasing geometry: efficiency estimates

The lasing region must be long and thin so that the induced emission is emitted preferentially in the direction of elongation. The width of the lasing region is constrained to be smaller than (or of order) the optical depth

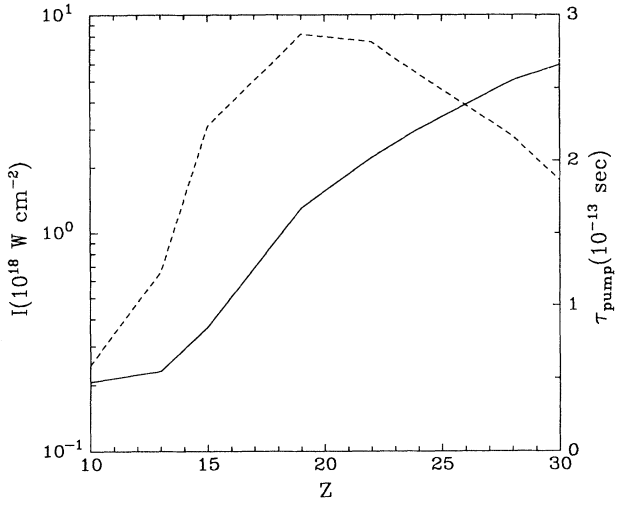

FIG. 10. Pump intensity I (W cm^{-2}) required to achieve maximum gain vs Z, as calculated from Eq. (48) (solid line), together with the corresponding required maximum pump-laser pulse length $\tau_{\rm pump}$ (sec), from Eq. (47) (dashed line).

of the $n = 2$ to 1 "dump" transition. The gain is spoiled if this photon is reabsorbed and electrons are excited to the $n = 2$ level. In colder material the $n = 2$ to 1 photon is absorbed in bound-free transitions. Thus the photons are absorbed in cold spheres that surround the hot lasing medium of spheres. It is clearly desirable to have a well-delineated width (of order the $n = 2$ to 1 optical depth) to the region which is heated by the pump laser. We have calculated the $n = 2$ to 1 optical depth numerically (see Sec. II). In Fig. 8(c) we plot τ_{12}^*, the number mean free paths in a sphere radius for the dump transition photon, at the instant of peak gain, for the optimum sphere, vs Z. We note from Eq. (20) that the optical depth is inversely proportional to $A_{21}\lambda_{21}^3 n_1 n_e Z^{-2} \propto Z^{-4} n_e n_1 \propto Z^{-4} x^{*-3}$, since $n_1 \sim 1$, for all Z. The single maximum in τ_{12}^* for $Z = 19$ results from the rapid decline in x^* between $Z = 10$ and 20, and its essentially constancy for larger Z [Fig. 8(b)].

The requirement that the dump photon escape freely imposes a rather small upper bound on the width of the amplifying region. The finite-width amplified spontaneous emission (ASE) beam will propagate out of the active region because of diffraction and also because of scattering on any density inhomogeneities which persist during the gain interval. In order to estimate these effects, we compute the lengths l_D and l_S for the ASE beam to diffract and to scatter out of the gain region. So long as these lengths exceed the gain length g_{32}^{-1} no auxiliary refocusing of the ASE beam is required.

The diffraction distance l_D is simply related to the width $R_\perp$ of the active region through

$$l_D = \frac{R_\perp^2}{\lambda_{ul}} \quad . \tag{50}$$

Individual scattering events are nearly forward because $\omega_{ul} \gg \omega_{pe}$ and $\lambda_{ul} \ll R$. Each results in a deflection in propagation angle $\Delta\theta \simeq (\Delta\omega_{pe}/\omega_{ul})^2$ with $\Delta\omega_{pe}$ the fluctuation in electron plasma frequency associated with a given density inhomogeneity Δn. We conservatively estimate $\Delta n \sim n$ with $n = n_0/x^{*3}$, the mean density. The angular width of the beam increases diffusively at a rate $D_\theta = (\Delta\theta)^2/l_{\rm spacing}$, with $l_{\rm spacing} = R_0 x^*$, the average intersphere spacing. The ASE beam scatters out of the active region in a distance $l_S = R_\perp/\theta$, where the accumulated angle $\theta = (D_\theta l_S)^{1/2}$. Combining results, we have

$$l_S = \left(\frac{R_\perp^2}{D_\theta}\right)^{1/3} \quad . \tag{51}$$

Using the relation $R_\perp = R_0 x^*/\tau_{12}^*$, we find that both $l_S g_{32}^*$ and $l_D g_{32}^*$ decrease with increasing Z, from $\sim 10^2$ for $Z = 10$ to $\sim 10^{-2}$ for Z = 30. Both become ~ 1 at $Z \simeq 20$. Therefore, above $Z = 20$, refocusing of the ASE beam is required to achieve gain.

The x-ray laser output intensity grows exponentially with the length of the lasing region l for l less than a critical length l_c. Specifically, for $l < l_c$, $I \sim \exp(g_{32} l)$. When $l = l_c$ the induced decay rate from level $n = 3$ is comparable with the spontaneous or collisional decay rate. The front of the laser pulse continues to be amplified for $l > l_c$, however, the response is no longer linear since the populations of the levels are affected by the laser light. The laser pulse tends to steepen and the intensity grows roughly linearly with length. At $l = l_c$ the laser intensity has the critical value $I_{\rm cr}$ at line center, where

$$I_{\rm cr} \sim 2.3 \times 10^{11}\, \bar{Z}^4 \bar{T}^{1/2} \left[\frac{n_3}{n_3 - g_3 n_2/g_2}\right] \text{W cm}^{-2} . \tag{52}$$

One may also estimate that $l_c \sim 2 g_{32}^{-1} \ln(\omega/l_c)$, where ω is the width of the lasing region.

Efficiency of the saturated amplifier can be appreciable. The input energy per ion is, roughly, $E_{\rm in} = Z(T + 2\langle E\rangle)$, where $\langle E\rangle$ is the average ionization energy per electron $\sim Z^2 E_{\rm H}/3$. The factor of 2 accounts for the radiation on average of one resonance photon per ionization event, which we assume, conservatively, to escape. At saturation, each ion contributes an energy $(5/36) b Z^2 E_H$ to the laser beam, taking account of the branching ratio b into level 3. With $T = Z^2 E_{\rm H}$, the resulting efficiency $b/(12Z)$ is seen to approach 1%.

The full dynamics of the laser propagation is complicated and we shall postpone any further discussion to a future publication. We note that it might be appropriate for some applications to make multiple parallel lasing regions simultaneously–this would effectively widen the total beam diameter but still keep the width of each "beamlet" narrower than the optical depth.

E. Propagation of the pump laser

Perhaps the simplest way to envisage heating the spheres with the picosecond pump laser is to produce a long focus and place the spheres in the focus (see Fig. 1). In this scenario the spheres in the focus will be heated and the shape of the lasing region is entirely defined by the focus. As we have already stated, the width of the lasing region is constrained to be less than the optical

depth of the $n = 2$ to 1 transition–this width is achievable at the focus of 0.25-μm light. Unfortunately, the scattering of light by the spheres broadens the focus and creates a problem. Let us first estimate this effect. We will consider alternatives subsequently. Let n_s be the density of spheres, R_0 the initial sphere radius, and R_f the sphere radius at maximum gain. We may wish to make $n_s \sim (8R_f^3)^{-1}$ so that the space is filled by the expansion and the gain is relatively uniform. The mean free path of the pump laser light is $\lambda_p \simeq (\sigma_{sc} n_s)^{-1}$ where the scattering cross section is given by Eq. (45). The length of the lasing region is effectively limited by λ_p. The total gain times length g_{tot} for a medium that is one mean free path long is

$$g_{tot} = (g_{32} R_0)\left(\frac{R_f}{R_0}\right)^3 \frac{1}{F(kR_0)} \quad , \tag{53}$$

where $F(kR_0)$ is defined in Eq. (45). Substituting numbers from our optimal cases into Eq. (53) we find $g_{tot} \simeq 15$ for $Z = 10$ ($\bar{Z} = 1$) and $g_{tot} \simeq 3 \times 10^{-3}$ for $Z = 30$. Since we would like $g_{tot} > 10$ for a moderately efficient laser we conclude that the scattering is intolerable at high Z.

There are several ways one might bypass the scattering problem–we will briefly mention two. The spheres could be placed in a narrow tube of width the optical depth. The pump laser would be focused into the tube and the scattered pump radiation would be reflected from the tube walls. The tube walls would, of course, become hot and expand, but in the time scale of interest this expansion is less than the width of the tube. A second possiblity is to use a line focus and illuminate the spheres perpendicularly to the direction of gain. Achieving high intensities with a line focus may be problematic. It is also difficult to imagine producing the very sharp gradient in sphere density needed in such a scheme.

Placing the spheres in the appropriate positions may not be too hard. If one just requires a cloud of spheres, one can suspend them by their thermal motions to an atmospheric scale height of approximately 50 μm. Alternatively, one may wish to drop the spheres into the path of the pump laser–on the picosecond heating time scale the spheres are stationary. Practical details such as these are really beyond the scope of this paper.

IV. CONCLUSIONS

This paper extends recombination laser schemes to shorter wavelengths. The crucial idea is to form a lasing medium from many submicrometer spheres. The spheres are heated by a powerful picosecond laser to temperatures comparable with the desired ionization energy. The material in a sphere is rapidly ionized and then, as the sphere expands and cools, it recombines. The desired nonequilibrium population inversion is obtained when the cooling rate is faster than the recombination rate. This cooling time is on the order of a picosecond and the size of the spheres is chosen to achieve such cooling times. Spheres are chosen chiefly because spherical expansions produce the most rapid cooling rates. Many spheres are needed to make a significant gain length product. A schematic of one arrangement of spheres and pump laser is given in Fig. 1.

We calculate the gain and other laser properties for lasing in the $n = 3$ to 2 transition in hydrogenlike ions. Ions with atomic numbers between 10 and 30 are considered. There is no reason why other lasing transitions might not be considered–we chose the simplest.

In Sec. II we consider the evolution of a single sphere. The expansion of the sphere is modeled (see Sec. II A) by an isothermal similarity model with a given initial temperature T_0 density, n_0, and radius R_0. A simple tractable model of the atomic physics is presented in Sec. II B. It is hoped that this model will aid understanding. In Sec. II C, we numerically calculate the gain with a more complete atomic model. The peak gain for a given Z is a function of T_0 and R_0. We calculate the optimum values of T_0 and R_0 (those values that produce the largest gain) for each Z. In Figs. 7(a)–7(c), we plot the optimum gain R_0 and T_0 against Z. The optimum gain falls rapidly from about 250 cm^{-1} for $Z = 10$ to about 0.1 cm^{-1} when $Z = 30$.

In Sec. III, we consider the issues involved in heating the microspheres with a picosecond laser. The isothermal assumption is justified in Sec. III A. In Sec. III B the absorption and scattering of the pump-laser by a sphere is calculated. The required pump-laser intensity is calculated in Sec. III C. The width of the lasing region is limited to be narrower than the optical depth of the $n = 1$ to 2 transition, as discussed in Sec. III D. Finally, in Sec. III E, we show that scattering of the pump laser beam limits the kinds of pumping schemes that are possible.

The considerations in this paper involve a number of physics processes and some of our models should be improved. In future work we intend to consider a more complete atomic model–specifically more ionization stages and more detailed calculations of the pump propagation. Specifically, we should include the heliumlike ion and model the ionization from the heliumlike state. Including the heliumlike ion will also provide a drain of the hydrogenlike ground state during recombination, thus reducing the $n = 1$ to 2 excitation. It may also be desirable to include the effect of a finite length heating pulse. Of course, better modeling of the spheres will lead to better estimates of the optimal sphere sizes and temperatures. The experimental implementation of this idea is relatively straightforward, although the pump-laser requirements are at the forefront of current technology. An important consideration is the reduction of prepulse to an acceptable level. Energy in a prepulse can create a uniform warm plasma before the main pulse arrives. This will destroy the scheme. There are many ways to reduce the prepulse and we hope to try some of them on the Princeton powerful subpicosecond laser in the future.

There are other possible uses of the microsphere "gas." For instance, coincidence pumping of one transition by another [20–22] requires the pump ion and the pumped ion to be in different plasma conditions. This could be achieved by making the spheres of the pump element a different size than the pumped element. The sizes of

the spheres are chosen so that they yield the appropriate plasma conditions upon heating and expanding. The spheres are intermingled and heated simultaneously by the pump laser. There are two advantages to this scheme. First, the geometric coupling of pump photons with lasing ions would be close to 100% in such a scheme. Second, the plasma conditions may be controlled with some precision by controlling the sphere sizes and the pump laser intensity.

In summary, we believe that the calculations presented here indicate that lasing can be achieved at wavelengths of 10 to 40 Å with our proposed scheme.

ACKNOWLEDGMENTS

We are happy to acknowledge stimulating discussions with Russell Kulsrud, Charles Skinner, Szymon Suckewer, and William Tighe. This work was supported by the United States Department of Energy under Contract No. DE-AC02-76-CHO-3073.

APPENDIX

Here we justify the use of expression Eq. (22) for the value of the line-shape function at line center. There are three contributions to the line-shape function: Doppler broadening, Stark broadening due to ions (quasistatic broadening), and Stark broadening due to electrons (impact broadening).

The principal source of Doppler broadening is the gradient in directed velocity over the plasma volume. As viewed along a ray passing through the sphere center, the Doppler shift is proportional to radius; see Eq. (3). Taking account of the radial dependence of the plasma density, Eq. (2), one obtains a Doppler profile of the form

$$S_d(\lambda) = \left(\frac{1}{2\pi}\right)^{1/2} \frac{1}{\Delta\lambda_d} \exp\left[-\frac{1}{2}\left(\frac{\lambda-\lambda_{ul}}{\Delta\lambda_d}\right)^2\right] \quad , \tag{A1}$$

where $\Delta\lambda_d$ is given in Eq. (23).

The ion quasistatic broadening results from the linear Stark shift of the energy sublevels of a given principal quantum number in the radiating ion caused by the electric fields of nearby ions. Ions typically move sufficiently slowly so that the level shifts can be assumed to be determined given the current electric-field strength, i.e., only the positions of the perturbing ions are required, and not their trajectories. When the shifts so computed are averaged over sublevels, each weighted by its contribution to the line intensity, and also over electric-field strengths due to the statistical distribution of ion positions, the result for the quasistatic width for transitions between levels n_u and n_l in hydrogenlike ion is[23]

TABLE I. Linewidth contributions at gain maximum.

	Linewidth at t^* (10^{-10} cm)				
Z	$\Delta\lambda_e$	$\Delta\lambda_d$	$\Delta\lambda_i$	T_0 (keV)	x^*
10	1.93	5.59	40.03	1.37	8.76
13	1.66	3.30	42.79	1.36	4.60
15	1.47	2.60	44.19	1.50	3.24
19	0.91	2.07	40.33	2.44	1.95
22	0.43	1.74	24.45	3.10	1.78
24	0.25	1.57	16.36	3.57	1.78
28	0.09	1.30	8.00	4.58	1.77
30	0.06	1.19	5.52	5.05	1.82

$$\Delta\lambda_i = \frac{8}{10^{2/3}} \left(\frac{Z_p}{Z_r}\right) \frac{\hbar}{mc} n_p^{2/3} \lambda_{ul}^2 \left(n_u^2 - n_l^2\right) \quad . \tag{A2}$$

Here Z_p and Z_r are, respectively, the net charge of the perturber and the nuclear charge of the radiator, and n_p is the perturber density. For our single species plasma, we take, to good accuracy, $Z_p = Z_r = Z$ and $n_p = n_e/Z$.

Electron broadening results from random phase shifts of the radiator wave function induced by the electric fields of passing electrons. The resultant line-shape function is Lorentzian and has a width [24]

$$\Delta\lambda_e = \frac{8n_e}{\pi c} \langle v \rangle \lambda_{ul}^2 \rho_0^2 \left[0.33 + \ln\frac{\rho_m}{\rho_0}\right] \quad . \tag{A3}$$

Here

$$\rho_0^2 = 18 \frac{e^4}{\hbar^2} \frac{1}{\langle v \rangle^2} \left(\frac{\hbar^2}{Zme}\right)^2 \tag{A4}$$

and

$$\rho_m = \left(\frac{T}{4\pi e^2 n_e}\right)^{1/2} = \lambda_D \quad . \tag{A5}$$

In order to estimate the relative importance of these effects, we present, in Table I, results for the various widths at the time t^* of maximum gain as a function of Z for optimum (R_0, T_0). In all cases

$$\Delta\lambda_i \gg \Delta\lambda_d > \Delta\lambda_e \quad . \tag{A6}$$

In the case of the H_α transition, there is a component of the line, with intensity 0.29 of the total [25], which has no linear Stark shift. For this component, the width is determined by convolving the Doppler and impact line-shape functions. Since the Doppler width is predominant, we neglect the impact contribution and obtain Eq. (22) at line center. A corresponding calculation for the L_α (dump) transition produces the same result for S, except that the relative intensity of the unshifted component is 0.67.

[1] S. Suckewer, C. H. Skinner, H. Milchberg, C. Keane, and D. Voorhees, Phys. Rev. Lett. **55**, 1753 (1985).
[2] D. L. Mathews *et al.*, Phys. Rev. Lett. **54**, 110 (1984).
[3] M. D. Rosen *et al.*, Phys. Rev. Lett. **54**, 106 (1984).
[4] S. Suckewer and C. H. Skinner, Science **247**, 1553 (1990).
[5] Assuming a bound-free absorption coefficient of order 10^{-19} cm^2. See, for example, C. W. Allen, *Astrophysical Quantities*, 3rd (Humanities Press, Atlantic Highlands,

NJ, 1973), p. 96.
[6] James H. Hunter, Jr. and Richard A. London, Phys. Fluids **31**, 3102 (1988).
[7] Ya. B. Zel'dovich and Yu. P. Raizer, *Physics of Shock Waves and High-Temperature Hydrodynamic Phenomena* (Academic, New York, 1966), Vol. 1, p. 406.
[8] G. J. Pert, J. Phys. B **23**, 619 (1990).
[9] L. M. Biberman, V. S. Vorob'ev, and I. T. Yakubov, Dokl. Akad. Nauk SSSR **296**, 576 (1987) [Sov. Phys.—Dokl. **32**, 753 (1987)].
[10] C. J. Keane, Ph. D. thesis, Department of Astrophysical Sciences, Princeton University, 1986.
[11] Hans. A. Bethe and Edwin E. Salpeter, *Quantum Mechanics of One- and Two- Electron Atoms* (Plenum, New York, 1977), p. 266.
[12] C. H. Nam, E. Valeo, S. Suckewer, and U. Feldman, J. Opt. Soc. Am. B **3**, 1199 (1986).
[13] A. I. Shestakov and D. C. Eder, J. Quant. Spectrosc. Radiat. Transfer **42**, 483 (1989).
[14] H. W. Drawin, Z. Phys. **225**, 483 (1969); H. W. Drawin, CEA–Euratom Report No. EUR-CEA-FC-383, 1966 (unpublished).
[15] *NAG Fortran Library, Mark 14*, NAG Inc., Downers Grove, IL, 1990, routine D02NBF (64-bit precision).
[16] S. I. Braginskii, in *Reviews of Plasma Physics*, edited by M. A. Leontovich (Consultants Bureau, New York, 1965), Vol. 1, p. 205.
[17] J. D. Jackson, *Classical Electrodynamics* (Wiley, New York, 1975).
[18] *Handbook of Mathematical Functions*, Natl. Bur. Stand. Appl. Math. Ser. No. 55, edited by M. Abramowitz and I. A. Stegun (U.S. GPO, Washington, DC, 1972), p. 435.
[19] See, for example, S. C. Wilks, W. L. Kruer, M. Tabak, and A. B. Langdon, Phys. Rev. Lett. **69**, 1383 (1992); X. Liu and D. Umstadter, *ibid.* **69**, 1935 (1992).
[20] B. A. Norton and N. J. Peacock, J. Phys. B **8**, 989 (1975).
[21] A. V. Vinogradov, I. I. Sobel'man, and E. A. Yukov, Kvant. Elektron. (Moscow) **2**, 105 (1975) [Sov. J. Quantum. Electron. **5**, 59 (1975)].
[22] K. J. Ilcisin, Ph. D. thesis, Department of Astrophysical Sciences, Princeton University, 1991.
[23] I. I. Sobel'man, *An Introduction to the Theory of Atomic Spectra* (Pergamon, New York, 1972), p. 420; see also Hans R. Griem, *Spectral Line Broadening by Plasmas* (Academic, New York, 1974).
[24] I. I. Sobel'man, *An Introduction to the Theory of Atomic Spectra* (Ref. [23]), pp. 428 and 429.
[25] Hans A. Bethe and Edwin E. Salpeter, *Quantum Mechanics of One- and Two-Electron Atoms* (Ref. [11]), p. 277.